Vol. 68: 73–89, 2016
doi: 10.3354/cr01383

CLIMATE RESEARCH
Clim Res

Published online April 14

Precipitation downscaling using the artificial neural network BatNN and development of future rainfall intensity-duration-frequency curves

Sze Miang Kueh*, King Kuok Kuok

Faculty of Engineering, Computing and Science, Swinburne University of Technology Sarawak Campus, Jalan Simpang Tiga, 93350 Kuching, Sarawak, Malaysia

ABSTRACT: This paper proposes an artificial neural network (ANN) approach to forecasting future precipitation through spatial downscaling and constructing new intensity-duration-frequency (IDF) curves that take climate change into consideration using a temporal downscaling method. For spatial downscaling, the bat neural network (BatNN) was developed and benchmarked with the traditional scaled conjugate gradient neural network (SCGNN). Both downscaling models were trained with observed precipitation series from Kuching and selected predictors from 1961 to 1990 (base period). Evaluations from goodness-of-fit metrics and QQ-plots from 1991 to 2010 showed that BatNN outperformed its benchmark in terms of predicting accuracy. However, both models showed an underestimation of extreme precipitation events. Subsequently, future precipitation forecasts made by BatNN were used as the basis for the construction of new IDF curves. A scaling-GEV (general extreme value) approach was used to temporally downscale the predicted daily annual maximum precipitation quantile into sub-daily quantiles. The feasibility of the approach was validated with observed precipitation and the Gumbel distribution method. Predicted future IDF curves for the 2020s, 2050s and 2080s showed an increase in precipitation extremes of 19% relative to the base period.

KEY WORDS: Artificial neural network · Statistical downscaling · Precipitation forecast · Intensity-duration-frequency curve · IDF curve

1. INTRODUCTION

Climate change has become a topic of general interest due to its impacts, such as heatwaves, drought and floods and has affected the well-being of mass society (Valipour 2015a,b). According to the IPCC fifth assessment report (AR5) working group 1, the global climate has been following a rising trend in temperature, averaging at 0.85ºC over the period from 1888 to 2012 (Hartmann et al. 2013). In addition, it has been reported that changes in extreme climate events can be traced back to the 1950s, when a decrease in the number of cold days and an increase in warmer days was recorded (Caesar & Lowe 2012, Orlowsky & Seneviratne 2012, Donat et al. 2013, Sillmann et al. 2013). Along with increasing global mean temperature, the IPCC (2013) has also reported, with medium confidence, that extreme events related to precipitation might have increased at the same time but these vary by region.

With regard to the change in precipitation (e.g. rainfall, snowfall, hail, drizzle and sleet) over land, some regions have experienced wetter conditions while others have become drier (Valipour 2015a). In the eastern areas of North and South America, it has become wetter and while the overall mean temperature has increased, the increment is smaller than elsewhere (IPCC 2013). On the other hand, in the northern lands where the climate is traditionally cold, more precipitation events can be observed. This

*Corresponding author: skueh@swinburne.edu.my

is due to the increased water-holding capacity of the atmosphere associated with warmer temperatures. In particular, Southeast Asia has experienced a temperature increase of up to 1ºC, and this is projected to rise by 1.5 to 2ºC in the 2050s relative to the observed mean temperature for 1986 to 2005 (IPCC 2013). As such, mean precipitation can be expected to increase across the region.

At present, future changes in climate variables are projected through global climate models (GCMs) produced by meteorological research centres. Unfortunately, these projections do not truly represent local weather conditions (typically under 5 km) as their scale is too large, ranging from 100 to 300 km. Therefore, weather scientists have been using spatial 'downscaling' techniques to bridge the resolution gap by connecting global and local weather conditions and quantifying the relationships between related climate variables. Fundamentally, there are 2 distinct categories of spatial downscaling: dynamical and statistical. The former involves the use of high resolution numerical models to nest the GCM into the regional climate model (RCM), while the latter focuses on deriving statistical relationships between the GCM and the local climate. This study will focus on the statistical downscaling approach as it is considered 'lighter' in terms of computational power and less time-consuming (Wilby & Wigley 1997).

In general, statistical downscaling can be classified into regression methods, weather typing and weather generators (Wilby & Wigley 1997, Fowler et al. 2007). Regression methods include the delta method, linear and multilinear regression, canonical component analysis (Barnett & Preisendorfer 1987) and artificial neural networks (ANNs). Weather-typing methods relate pre-determined weather classes to local and regional climate variables (Wilby & Wigley 1997). The methods used for classifying weather types include empirical orthogonal functions (EOF) or principal component analysis (PCA) (Goodess & Palutikof 1998), sea level pressure indices (Conway et al. 1996), cluster analysis (Fowler et al. 2000) and fuzzy rules (Bárdossy et al. 2002). Weather generators are statistical models capable of reproducing attributes of climate. They are usually used to create synthetic time series of climate variables, such as precipitation and temperature. Some widely used weather generators are the Long Ashton Research Station Weather Generator (LARS-WG) and the Statistical Downscaling Model (SDSM) of Wilby et al. (2002). In the present study, statistical downscaling using a metaheuristic ANN is considered.

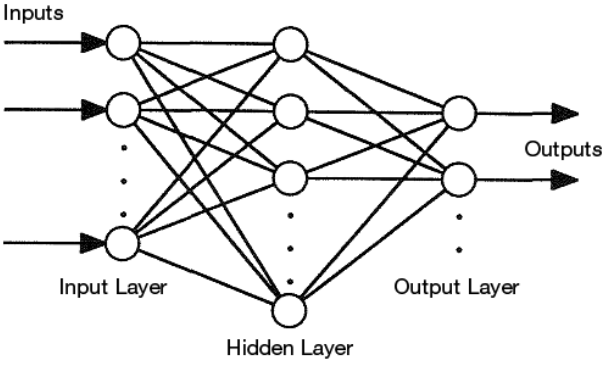

Fig. 1. Overview of the structure of an artificial neural network (ANN) (Dawson & Wilby 1998)

ANNs are known as 'black box' mechanisms as they mimic the biological processes of an animal brain, or more specifically, the neural structure of the cerebral cortex of a human brain. The basic structure of an ANN is shown in Fig. 1. ANNs are capable of analysing nonlinearities in a dynamical model that impede an exactly solvable solution, particularly in meteorology, where the atmospheric parameters are highly nonlinear and an understanding of the physical processes is lacking (Luk et al. 2000).

According to French et al. (1992) and Lachtermacher & Fuller (1994), the advantages of using ANNs compared to other statistical models are: (1) ANNs do not require *a priori* knowledge of the underlying process; (2) ANNs include all relationships controlling the process; and (3) ANNs do not require pre-specified parameters and, therefore, are not limited by such conditions. In comparison, traditional statistical methods rely on inherent assumptions that limit their applicability. For example, multilinear regression assumes that parameters are linear, while polynomial regression requires pre-determined parameters. Marzban & Stumpf (1996) have argued that the incorporation of assumptions may impede the predictive capabilities of a particular forecasting model.

In addition, ANNs are flexible enough to be adapted to a wide range of problems, in which the number of hidden nodes can be adjusted to suit the complexity of a particular model (Luk et al. 2000). Valverde Ramírez et. al (2005) compared the abilities of an ANN and multi-linear regression to forecast precipitation in the São Paulo region and found that the ANN performed better than its counterpart. A study by Silverman & Dracup (2000) proved the viability of ANNs in predicting long-range precipitation. Karamouz et al. (2009) also successfully predicted long-term precipitation using an ANN, though they

commented that the results required more fine-tuning to achieve the desired accuracy.

In general, training of ANNs (the process through which weights and biases are assigned and optimised) is implemented through gradient-based backpropagation methods, such as scaled conjugate gradient (SCG) (Møller 1993) and Levenberg-Marquardt (LM) (Levenberg 1944, Marquardt 1963). Unfortunately, these gradient-based methods are easily trapped within a local optimum point, which is undesirable because it prevents the network searching for the global optimum. As such, the aim of the present study was to implement a metaheuristic algorithm, well-known for their ability to avoid local trappings, as the ANN training function.

Metaheuristic algorithms have gained recognition through solving realistic engineering problems in various fields such as hydrology, geotechnical and structural engineering (Gandomi et al. 2013). The advantage of metaheuristics is that it makes few assumptions about the problem being solved and is, therefore, applicable to a variety of problems (Blum & Roli 2003). The metaheuristic algorithm used here is the bat algorithm (Yang & Gandomi 2012). It is scripted and implemented as an ANN optimisation function and can be run through the MATLAB ANN toolbox. The trained network can then be used to make predictions for long-term future precipitation scenarios in 3 multi-decadal periods, namely the 2020s (2011 to 2040), 2050s (2041 to 2070) and 2080s (2071 to 2100). Future intensity-duration-frequency (IDF) curves can then be constructed from these predictions.

IDF curves provide valuable information about the estimated intensity of a precipitation event for a given duration. Hydrologists depend on IDF curves to design suitable stormwater management infrastructures based on a specified return period within a catchment. IDF curves can be constructed based on, but not limited to, estimations from observational data, typically in an annual maxima series (AMS). The AMS is ranked and sorted in descending order. The exceedance probability, which is the probability of precipitation of a higher magnitude than the corresponding data, is assigned to each of the sorted AMS. It can be calculated using the plotting position formula and the return period can then be obtained from the inverse of the exceedance probability. The process is then repeated for other durations. Finally, IDF curves can be constructed by plotting the intensity, represented by the sorted AMS, along with its corresponding return periods against duration, typically measured in minutes.

Various studies (Arnbjerg-Nielsen 2012, Alam & Elshorbagy 2015) have reported that climate change exerts an increasing trend towards the maximum amount of daily and sub-daily precipitation. From the hydrology perspective, such change has the potential to affect the intensity, duration and frequency of precipitation estimates. This implies that the hydrologic design of stormwater management systems should be changed. As the current design standard of stormwater management uses historically based IDF curves, which are expected to change, it is crucial that immediate attention is given to projections of future precipitation, particularly daily and sub-daily precipitation in the context of climate change.

Updated IDF curves that account for climate change have been put forward by Nguyen et al. (2008) for Quebec, Canada, Solaiman & Simonovic (2011) for London, England, Hailegeorgis et al. (2013) for Trondheim, Norway and Rodríguez et al. (2014) for Barcelona, Spain. Unfortunately, there is still lack of studies related to updating IDF curves in Malaysia. Hence, in consideration of possible changes in IDF curves due to climate change, we propose a statistical method for the temporal downscaling of precipitation forecasts produced by spatial downscaling models. This temporal downscaling method will enable sub-daily precipitation to be estimated for the construction of new IDF curves in the context of climate change.

Throughout the paper, it is assumed that the readers are familiar with the basics of ANNs (see Maren et al. 1990, Masters 1993, Flood & Kartam 1994, Hassoun 1995, Rojas 1996). The ANN materials covered are strictly focused on feedforward networks, as these have been used extensively for simulation and forecasting of water resources (Maier & Dandy 2000).

2. MATERIALS AND METHODS

2.1. Study area

As a tropical country located near the Equator, Malaysia is a considerably wet country with annual total precipitation of 3500 mm in Peninsular Malaysia (West Malaysia) and up to 4000 mm in Sabah and Sarawak (East Malaysia). Though the 4 seasons are not present in Malaysia, the local climate can be distinguished into 2 monsoons: Northeast (NE) and Southwest (SW). The former spans from November to March and the latter from May to September. Historically, the NE monsoon has been a wet season with an expected maximum daily precipitation of 350 to

480 mm. On the other hand, the SW monsoon is relatively dry, with a maximum daily precipitation of 42 to 57 mm.

The climate of Peninsular and East Malaysia differ, in that the latter generally receives a higher precipitation volume, especially during the NE monsoon. The area used for study is Kuching (1° 33′ N, 110° 20′ E; Fig. 2). The average total precipitation in Kuching is about 4096 mm annually (based on precipitation data from 1958 to 2010). Kuching typically experiences maximum precipitation during the end of December and early January; while minimum precipitation events occur during June and July (MOSTI 2013), when the maximum daily precipitation can reach up to 485.4 mm. Fig. 3 shows an isohyet of mean seasonal precipitation distribution during 1960 to 1990 throughout East Malaysia. As the figure shows, Kuching is the wettest area within the region.

Fig. 2. Location of Kuching (sourced from Google Maps)

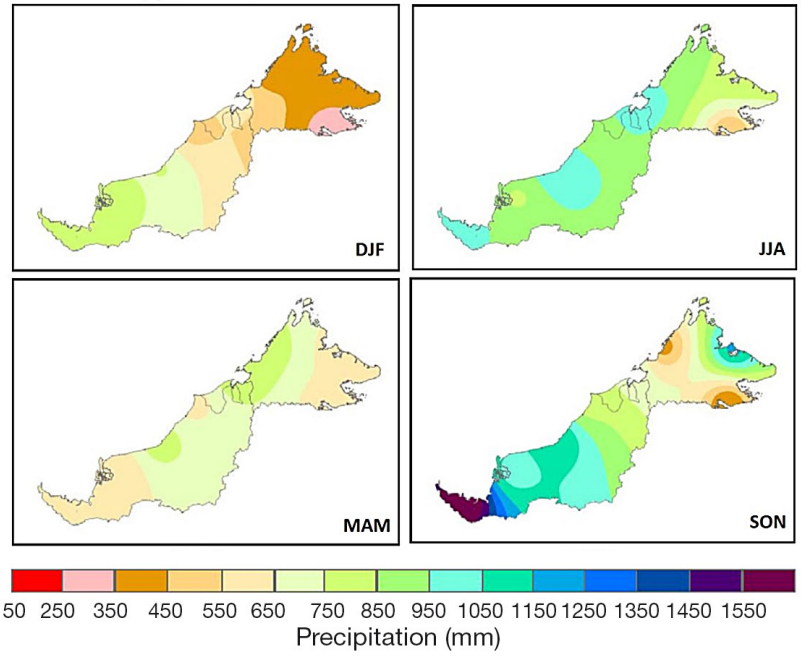

Fig. 3. Mean seasonal precipitation in East Malaysia from 1961 to 1990 (adapted from Malaysian Meteorological Department [MMD] 2009). DJF: December, January, February; MAM: March, April, May; JJA: June, July, August; SON: September, October, November

2.2. Climate model

The GCM model selected for this study is ECHAM5, developed at the Max Planck Institute for Meteorology (MPIM), Germany. It is an atmosphere–ocean coupled GCM, with a resolution of approximately 1.875° latitude (Lat.) × 1.875° longitude (Long.). Further details on ECHAM5 have been documented by Roeckner et al. (2003). The predictors are downloadable from the IPCC data distribution centre (www.ipcc-data.org/sim/gcm_monthly/SRES_AR4/index.html) in GRIB and netCDF file formats. There are 3 ensemble runs available for download, and 'run 3' was chosen for this study as it contains the most complete predictor sets compared to its counterparts. In general, there are 4 distinct types of climate scenarios available, namely A2, A1, B2 and B1. These scenarios are based on the 'Special Report on Emission Scenarios' (SRES) and have been used as the baseline setting for most GCMs, including ECHAM5.

The reasons for selecting ECHAM5 are its availability and completeness of data, as well as better resolution compared to its counterparts. For example, HadCM3 (Hadley Centre for Climate Prediction and Research, Met Office, UK) has a resolution of 2.5° Lat. × 3.75° Lon. and CGCM3.1 (T47) (Canadian Center for Climate Modelling and Analysis, Canada) has a resolution of 3.75° Lat. × 3.75° Lon. In addition, a study by Salathe et al. (2007), which presented an evaluation of 10 GCMs based on 20th century simulations in the Pacific Northwest, USA, found the ECHAM5 model to be a good 'middle-of-the road' scenario. This climate model also shows relatively small biases in temperature and precipitation simulation for the 20th century compared to other GCMs, which include HadCM3, CCGCM3.1, CSIRO-Mk3

(Commonwealth Scientific and Industrial Research Organisation, Australia) and GISS-ER (Goddard Institute for Space Studies, NASA, USA), as well as NCEP/NCAR reanalysis data.

This model was used by Cheng et al. (2008) in their study of daily climate scenarios in south-central Canada, Sunyer et al. (2012) in assessing a regional climate model based on ECHAM5 for extreme precipitation estimation in Copenhagen and Gutiérrez et al. (2013) in assessing statistical downscaling techniques in Spain. Like any other GCM, ECHAM5 has limited use in modelling processes at a finer resolution, which is mainly required for hydrological impact assessments. Therefore, it is necessary to conduct spatial downscaling.

2.3. Data

A statistical downscaling model usually relies on 2 types of data, which are the predictand (to be predicted) and predictors (to predict). Locally observed climate variables, such as temperature or precipitation, are typically used as the predictand. The predictand for the current study consisted of observed precipitation data from 1961 to 2010, obtained from the Kuching Airport rainfall gauge station. The data was divided into 2 subsets: 1961 to 1990 for training and 1991 to 2010 for cross-validation. It should be noted that the subset data used for cross-validation should not be included in the input during the training stage, else all solutions are given to the ANN and there is no point in evaluating the results. The MATLAB ANN toolbox was used as the operating platform for BatNN.

It should be noted that reanalysis data were not used in the present study due to lack of data for the studied area. This method can be classified as a model output statistics (MOS) approach (Maraun et al. 2010). The MOS method involves approaches that develop empirical relationships between the observed predictand and large-scale predictors produced by climate models. GCM control runs have been applied for spatial downscaling by Conway et al. (1996), Semenov & Barrow (1997), Sailor et al. (2000), Wilby & Wigley (2000), Huth et al. (2001), Frei et al. (2006) and Schoof & Robeson (2015).

Predictors consist of large-scale climate variable data, typically generated by GCMs. In the present study, predictors from ECHAM5 were downloaded from IPCC. The downloaded data consist of a '20C3M' simulation of 20th century climate from 1961 to 2000, and SRES A2, A1B and B1 projections of large-scale predictors for 2001 to 2100. All downloaded predictors are represented in monthly averaged values. Preliminary correlation tests between predictors of these scenarios for 2001 to 2010 showed that SRES A2 had slightly better correlation with the precipitation in Kuching. SRES A2 was found to be better at reproducing the mean higher intensity precipitation compared to A1B and B1, and was therefore chosen as the representative scenario for Kuching. As a brief background on SRES A2, this emission scenario is known as the worst case scenario for future climate change as it follows a path of increasing carbon dioxide (CO_2) throughout the 21st century. Further details of SRES A2 and other scenarios have been documented by Nakicenovic & Swart (2000).

A list of available predictors, as well as their respective correlation with local observational precipitation, is shown in Table 1. Note that some predictors do not contain data for the study area, and are therefore omitted from the list. As there were 18 types of predictor available for the current study site, it was crucial to analyse the correlations between the predictors and local precipitation because selecting predictors with high correlation as input can reduce 'noise' within the model (Gorp et al. 1998). Screening of predictors based on correlation with the local climate has been performed by researchers in different regions, most notably Wilby

Table 1. Correlation coefficient, r, and p-value of ECHAM5 20C3M predictors

ECHAM5 predictors		r	p
Code	Description		
pr	Precipitation flux	−0.151	0.001
hur850	Relative humidity at 850 hPa	−0.544	0
hur500	Relative humidity at 500 hPa	−0.114	0.013
hur200	Relative humidity at 200 hPa	−0.544	0
ts	Surface skin temperature	0.624	0
tas	Air temperature at 2 m	0.624	0
uas	Zonal wind speed	0.024	0.593
vas	Meridional surface wind speed	−0.275	0
ta850	Air temperature at 850 hPa	0.614	0
ta500	Air temperature at 500 hPa	0.583	0
ta200	Air temperature at 200 hPa	0.545	0
ua850	Zonal wind at 850 hPa	0.171	0
ua500	Zonal wind at 500 hPa	0.001	0.68
ua200	Zonal wind at 200 hPa	0.075	0.1
psl	Air pressure at sea level	0.067	0.143
va850	Meridional wind at 850 hPa	−0.350	0
va500	Meridional wind at 500 hPa	0.134	0.03
va200	Meridional wind at 200 hPa	0.077	0.09

et al. (2003, 2006), Diaz-Nieto & Wilby (2005), Haylock et al. (2006), Wetterhall et al. (2006), Wilby & Harris (2006), Fowler & Wilby (2007), Dibike et al. (2008), Hashmi et al. (2011) and Wilby & Dawson (2013). In addition, the use of too many predictors often results in overfitting (Kuligowski & Barros 1998). A p-value test with a significance level of 0.05 was used in order to determine the significance of the correlation test results.

Table 1 gives the correlation coefficient, r, and the p-value for a list of available predictors for the ECHAM5 model. A negative r value signifies that the predictor is inversely correlated with precipitation in Kuching. Based on the correlation test results, it was decided that predictors with $r > 0.4$ and $p < 0.05$ would be used as input. In this case, they were ts, tas, ta850, ta500, ta200, hur850 and hur200. Along with the selected predictors, monthly precipitation series from the same period (1961 to 1990) were included as the input for training ANN models.

The precipitation predictor of ECHAM5 20C3M (pr) was found to be unable to capture the characteristics of the local precipitation. Fig. 4 provides a profile of the precipitation simulated by ECHAM5 20C3M (denoted as 'pr') along with the observed precipitation from Kuching (denoted as 'OBS') from 1961 to 2000. There are several important features shown in the figure. (1) Monthly pr has an overall higher mean compared to OBS. (2) pr underestimates several extreme precipitation events. (3) pr has higher minimum and lower maximum precipitation than OBS. (4) OBS shows a distinct wave-like pattern in the form of continuous 'U' shapes, while pr does not describe such a pattern. Hence, pr is not a good predictor of Kuching precipitation.

2.4. Spatial downscaling approach using BatNN

This paper proposes BatNN as a method of spatial downscaling. It is a combination of an ANN and the bat algorithm (BA), where BA is used as the optimisation method for the ANN training. In order to validate the feasibility of BatNN and its advantages over the traditional ANN downscaling model, a benchmark, SCGNN, was used. SCGNN is based on the conventional scaled conjugate gradient optimisation algorithm. The workflow of spatial downscaling using the ANN is illustrated in Fig. 5. The input for the downscaling models are the predictors selected in Section 2.3 and observed precipitation data from Kuching for 1961 to 1990. This 30 yr period has been used widely in climatological applications as the reference or base period. A 30 yr period is able to capture most of the interannual and short time-scale variability within the climate system (IPCC 2011). In addition, the 1961 to 1990 period generally has good observed data (IPCC 2011).

The trained models were tested for their prediction accuracy by comparing their simulation to actual precipitation from 1961 to 1990. During this process, the optimal configuration settings for each downscaling model was determined via trial and error. If the results of a particular model were not satisfactory, the model was trained again with some adjustment made to its parameters, such as increasing or decreasing the number of hidden nodes (HN). The term 'satisfactory' refers to results that are not too far off from the results of other models.

In order to assess the prediction accuracy of each downscaling model, predicted precipitation outside of the training range was compared with observed precipitation. This validation process was conducted

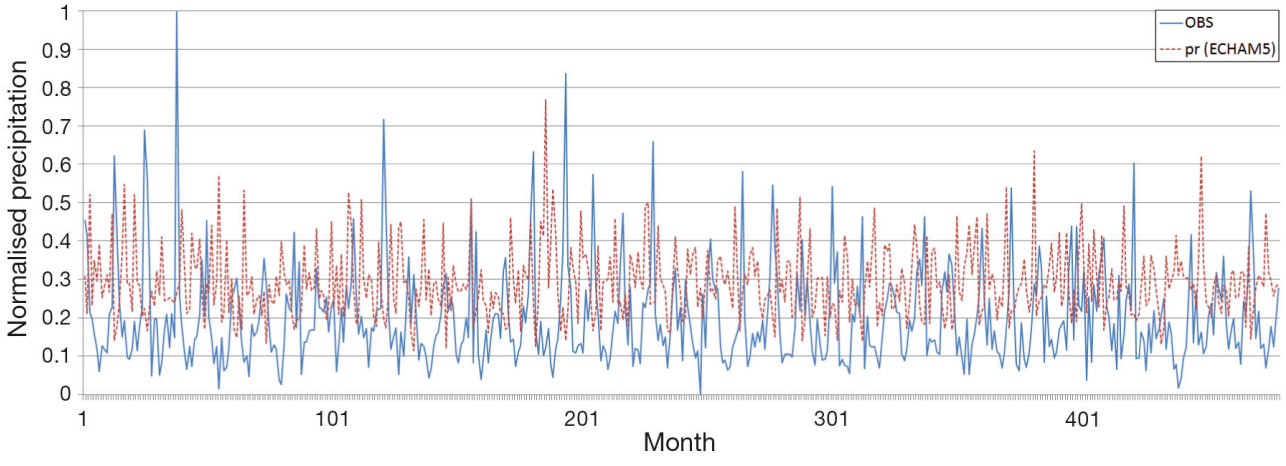

Fig. 4. Normalised observed (OBS) and ECHAM5 20C3M-produced (pr) monthly precipitation in Kuching from 1961 to 2000

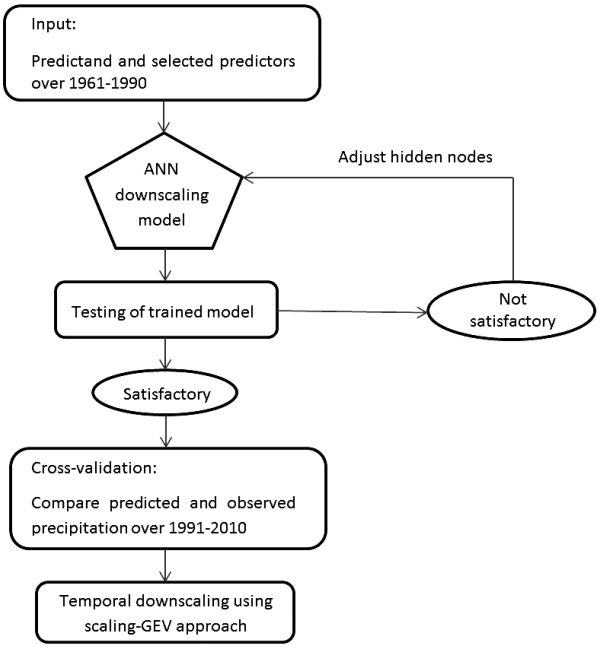

Fig. 5. Workflow for spatial downscaling using an artificial neural network (ANN). GEV: general extreme value

for 1991 to 2010. Finally, the trained models were inputted with large-scale projections of future climate variables in order to predict future precipitation. The predicted precipitation was then temporally downscaled to obtain precipitation series of shorter duration.

2.4.1. Bat algorithm (BA)

BA was originally developed by Yang (2010). The simplified BA can be downloaded from www.mathworks.com/matlabcentral/fileexchange/37582-bat-algorithm--demo-. It should be noted that the original version is not incorporated as a training algorithm for ANNs, but has been implemented as such in this study. The main idea behind the algorithm is the echolocation ability of bats for communication, navigation and predatory purposes. As bats live in dark areas, they rely on soundwaves or sonar to navigate around obstacles as well as to determine the size of objects (Richardson 2008). When encountering small prey, bats will raise the frequency of their sonar and reduce its loudness to a constant minimum (Møhl 1988, Surlykke et al. 2009). The following rules were used by Yang (2010) in developing the algorithm:

(1) Bats use echolocation to sense distance and have the ability to differentiate between prey and obstacles.

(2) Bats fly with random velocity (v_i) at position (x_i). Their sonar has a fixed minimum frequency (f_{min}) with varying wavelength (λ) and loudness (A_i) when searching for prey. Bats have the ability to adjust their sonar frequency and the rate of pulse emission (R_i) in relation to the proximity of their target. Normally, A_i will decrease as the bat gets nearer to its prey; while R increases to improve its accuracy (Lin et al. 2012).

(3) The loudness of sonar is assumed to vary from a large A_0, to a minimum but constant A_{min}.

The behavioural pattern of bats can be expressed as a pseudo-code (Fister et al. 2013):

1 Objective function f(x), $x = (x_1, ..., x_d)^T$
2 Initialise bat population x_i and v_i for $i = 1..n$
3 Define pulse frequency $Q_i \in [Q_{min}, Q_{max}]$
4 Initialise pulse rates, R_i, and loudness, A_i
5 While ($t < T_{max}$) // number of iterations
6 Generate new solutions by adjusting frequency
7 Update velocities and locations/solutions
8 If (rand(0,1) > R_i)
9 Select a solution among the best solutions
10 Generate a local solution around the best solution
11 End if
12 Generate a new solution by flying randomly
13 If (rand(0,1) < A_i and f(x_i) < F(x))
14 Accept the new solutions
15 Increase R_i and reduce A_i
16 End if
17 Rank the bats and find the current best
19 End while

BA has been applied in almost every area of optimisation, classification, image processing, feature selection, scheduling and data mining (Yang 2013). The algorithm is capable of efficiently solving nonlinear problems and finding optimal solutions (Yang 2011, 2012, Yang et al. 2012, Yang & Gandomi 2012). Musikapun & Pongcharoen (2012) and Ramesh et al. (2013) have found BA to be superior in multi-scheduling problems and combinatorial optimisation, respectively. In the field of imagery processing, a study on full-body human pose estimation by Abdel-Rahman et al. (2012) concluded that BA is better than particle swarm optimisation (PSO), particle filter (PF) and annealed particle filter (APF). As BA has yet to be incorporated into climatological studies, this paper intends to bridge the gap by utilising BA for statistical downscaling of climate variables.

2.4.2. Modifications to BA

The original BA fixes R_i and A_i at 0.5 throughout the training process. Such a simple approach does

not encompass the full extent of the predatory behaviour of bats. Therefore, R_i has been modified to be low enough, while A_i has been set to be high enough during the initial stage to fully exploit the search space. As more iterations pass, A_i gradually decreases while R_i increases in order to perform a local search. This emulates the predatory pattern of a bat, where it emits soundwaves, via screeches, with noticeable loudness but at a lower pulse rate to navigate and seek out prey. Once prey has been identified, the bat emits nearly inaudible soundwaves at a considerably higher pulse rate in order to pinpoint its prey and hunt. Eqs. (1) and (2) are simple mathematical representations for the processes of R_i and A_i, where both parameters automatically update themselves as the bat gets nearer to the prey (desired solution):

$$R_i = 1 - (0.9 \exp[-\alpha i_n]) \quad (1)$$

$$A_i = 0.9 \exp(-\alpha i_n) + 0.1 \quad (2)$$

where α = velocity factor and i_n = nth iteration (n = 1, 2, 3….).

In the present study, the velocity factor, α has been set to 0.001. It is a control parameter used to determine the rate of change for A_i. Higher α will lead to faster change of A_i, while lower α will lead to slower change of A_i.

In addition, Lévy flight was implemented to generate new random solutions, as opposed to the random solution generation mechanism of BA, shown in Line 12 of the pseudo-code. The benefits of Lévy flight have been studied by Viswanathan et al. (1996). In general, the mechanism helps to reduce the probability of returning to previously visited solutions, hence avoiding ineffectual searches and increasing the convergence rate. Above all, the modifications presented here will enable the algorithm to self-update the 2 controlling parameters based on the predatory behaviour of bats.

2.4.3. SCGNN as benchmark

In order to evaluate the feasibility of the proposed BatNN method, we used an alternative ANN that employs a scaled conjugate gradient (SCG) optimisation algorithm as the benchmark. This algorithm is a built-in feature of the MATLAB ANN toolbox. The SCG algorithm is a form of the gradient-descent method with the advantage of a faster convergence speed than the normal gradient descent, as it uses a step-size scaling technique to avoid line searching during iterations, which normally requires a lot of time (Møller 1993). It is commonly used as the learning algorithm for ANN training due to its simplicity and low resource consumption. Furthermore, SCG is not controlled by any particular parameter, hence does not require supervision or parameter manipulation. However, like all gradient-descent methods, the major flaw of this method is the tendency to be trapped within local optima, especially for problems with multiplane error surfaces.

2.4.4. Goodness-of-fit evaluations

There are various goodness-of-fit measuring metrics used by statistical modellers to determine the accuracy and efficiency of a particular model. However, each has its own weaknesses. For example, mean square error (MSE) and root mean square error (RMSE) tend to place heavier weight on large outliers due to the mathematical procedure of squaring errors, thereby influencing the total error of sample data. One plausible way of making allowance for the inherent weaknesses of accuracy metrics is to include >1 evaluation method. As such, in this study, the evaluations used to measure the accuracy of each model are the correlation coefficient, otherwise known as Pearson's product moment correlation coefficient (r), RMSE, mean absolute error (MAE), mean bias (MB) and the Nash-Sutcliffe model efficiency coefficient (E). Formulas for these evaluation metrics are as follows:

$$r = \frac{N\left(\sum_{i=1}^{N} O_i S_i\right) - \sum_{i=1}^{N} O_i \sum_{i=1}^{N} S_i}{\sqrt{\left[N\sum_{i=1}^{N} O_i^2 - \left(\sum_{i=1}^{N} O_i\right)^2\right]}\sqrt{\left[N\sum_{i=1}^{N} S_i^2 - \left(\sum_{i=1}^{N} S_i\right)^2\right]}} \quad \text{(Ideal = 1.0 or −1.0)} \quad (3)$$

$$\mathrm{RMSE} = \sqrt{\frac{\sum_{i=1}^{N}(O_i - S_i)^2}{N}} \quad \text{(Ideal = 0.0)} \quad (4)$$

$$\mathrm{MAE} = \frac{1}{N}\sum_{i=1}^{N}|O_i - S_i| \quad \text{(Ideal = 0.0)} \quad (5)$$

$$\mathrm{MB} = \frac{1}{N}\sum_{i=1}^{N}(O_i - S_i) \quad \text{(Ideal = 0.0)} \quad (6)$$

$$E = 1 - \frac{\sum_{i=1}^{N}(O_i - S_i)^2}{\sum_{i=1}^{N}(O_i - \bar{O}_i)^2} \quad \text{(Ideal = 1.0)} \quad (7)$$

where N is the total number of data, O_i = observed values, S_i = predicted values and $\bar{O}_i$ = mean of observed values

2.5. Temporal downscaling using the scaling-general extreme value method

Traditionally, IDF curves are constructed by fitting probability distributions onto annual maximum precipitation (AMP) series or partial duration series (PDS). However, the drawbacks of such methods are the fitting of distribution and estimation of parameters for different return periods as well as the extrapolation of results into different durations (e.g. 30 min, 1 h, 3 h). Work by Nguyen et al. (2002) and Willems & Vrac (2011) has described the scale invariance of precipitation, which uses a simple scaling approach to temporally downscale sub-daily precipitation from daily precipitation series. A scale invariance property means that precipitation properties are related to each other by a simple ratio (Gupta 2004). Essentially, the method is an application of a scaling parameter to the general extreme value (GEV) to estimate extreme precipitations for sub-daily duration (e.g. 30 min and 1 h). In the present study, a scaling-GEV approach was adopted to obtain future sub-daily precipitation from forecasted daily extreme precipitation series simulated by BatNN. The following paragraphs detail the procedure and equations related to scaling-GEV.

In general, GEV distribution corresponding to a return period τ can be expressed as:

$$X_\tau = \xi + \frac{\alpha}{\kappa}\{1-[1-LN(p)]^\kappa\} \quad (8)$$

where X_τ = GEV distribution of return period τ, p = probability of exceedance and α, κ and ξ are the location, scale and shape parameters, respectively.

Through the derivation of non-central moments (NCMs) of the GEV distribution shown below, it is possible to approximate the 3 GEV parameters (Nguyen et al. 2002):

$$\mu_k = \left(\xi + \frac{\alpha}{\kappa}\right)^k + (-1)^k\left(\frac{\alpha}{\kappa}\right)\Gamma(1+kx) + k\sum_{i=1}^{k-1}(-1)^i\left(\frac{\alpha}{\kappa}\right)^i\left(\xi+\frac{\alpha}{\kappa}\right)^{k-1}\Gamma(1+ik) \quad (9)$$

where k = order of NCMs ($k = 1, 2, 3$) and Γ = gamma function.

The relationship between the NCMs of the GEV distribution and the variable x can be expressed as:

$$\mu_k = \alpha(k)x^{\beta k} \quad (10)$$

where $\alpha(k) = E\{f^k(1)\}$ and $\beta(k) = \beta^k$ for simple scaling.

The assumption that the precipitation process is a simple scaling function is valid when the log-log plot of NCM versus duration is linear. Otherwise, the precipitation process is assumed to consist of multi-scaling functions (Gupta & Waymire 1990) in which the log-log plot will display a non-linear function. The slope of the linear function is known as the scaling exponent, β. Additionally, if there are 2 values of β, this means that the precipitation process displays 2 scaling behaviours. The point where the 2 scales meet is identified as the break-point. Finally, the linking of larger duration t to smaller duration λt can be achieved by the following equations (Nguyen et al. 2007):

$$\begin{aligned}\kappa(\lambda t) &= \kappa(t)\\ \alpha(\lambda t) &= \lambda^\beta\alpha(t)\\ \xi(\lambda t) &= \lambda^\beta\xi(t)\\ X_\tau(\lambda t) &= \lambda^\beta X_\tau(t)\end{aligned} \quad (11)$$

where λ^β is a simple scaling ratio obtainable through the division of the first order NCM of durations t and λt. Using the scaling-GEV method discussed in this section, forecasts of future daily AMP can be downscaled to sub-daily AMPs.

3. RESULTS AND DISCUSSION

3.1. Performance of BatNN

To obtain a final agreeable result, 100 simulation runs for both BatNN and SCGNN were carried out and recorded. The results presented in this section are the mean of these 100 simulations. Both ANN models were trained using 100 hidden nodes, 1000 iterations and a learning rate of 1. During the experiment, it was found that although SCGNN was faster in terms of convergence speed, it tended to either overfit or become trapped within a local optimum point. By contrast, BatNN could avoid local optima as it has the ability to conduct a global search (refer to Lines 12 to 14 of the BA pseudo-code in Section 2.4.1). This global search feature allows BatNN to abandon local optimum points when a new solution with better performance is found.

Table 2 shows the goodness-of-fit between BatNN and SCGNN predicted precipitation for 1991 to 2000 and 2001 to 2010. Both models showed comparable r-values. BatNN displayed better RMSE, MB and *E*-values compared to SCGNN. During simulation runs of SCGNN, about 67% of the results were discarded due to premature termination of training by the model. This is because SCGNN was constantly trapped within local optima, thereby causing the solution to converge prematurely.

Fig. 6 shows the QQ-plots of predicted against observed mean monthly precipitation for the 2 decades 1991 to 2000 and 2001 to 2010. It can be seen

Table 2. Goodness-of-fit for BatNN and its benchmark, SCGNN (scaled conjugate gradient neural network), for 1991 to 2000 and 2001 to 2010. RMSE: root mean square error; MAE: mean absolute error; MB: mean bias; *E*: Nash-Sutcliffe model efficiency coefficient

Downsca. model	Validation period	r	RMSE	MAE	MB	*E*
BatNN	1991–2000	0.97	1.38	1.19	−0.37	0.88
	2001–2010	0.95	2.02	1.7	−0.81	0.87
SCGNN	1991–2000	0.94	1.73	0.4	−0.1	0.82
	2001–2010	0.96	2.08	1.39	1.2	0.86

that both models were able to predict, with acceptable accuracy, precipitation events of lower intensity. However, BatNN and SCGNN showed underestimation of higher intensity precipitation, especially on the extremes. The underestimation was more profound in SCGNN. This can be attributed to the parameterisation schemes employed by the underlying GCM (Maraun 2012, 2013).

3.2. Predicted future precipitation and IDF curves

A dataset of 100 daily precipitation series for Kuching from 1961 to 2010 were simulated by BatNN based on ECHAM5 SRES A2. The average values were extracted to represent the final simulated daily AMP, as shown in Fig. 7. The simulated daily AMP displayed good agreement with observed daily AMP, as is evident in the QQ-plot shown in Fig. 8. However, there was a slight underestimation, of about 16.9 mm, of the most extreme precipitation event. The observed extreme was 485.4 mm while the simulated extreme was 468.5 mm.

3.3. Temporal downscaling through the scaling-GEV approach

In order to examine the scaling properties of the AMP in Kuching, analyses were conducted on the first 3 orders of NCMs. The log-log plot for Kuching (Fig. 9) shows the scaling relationships for all dura-

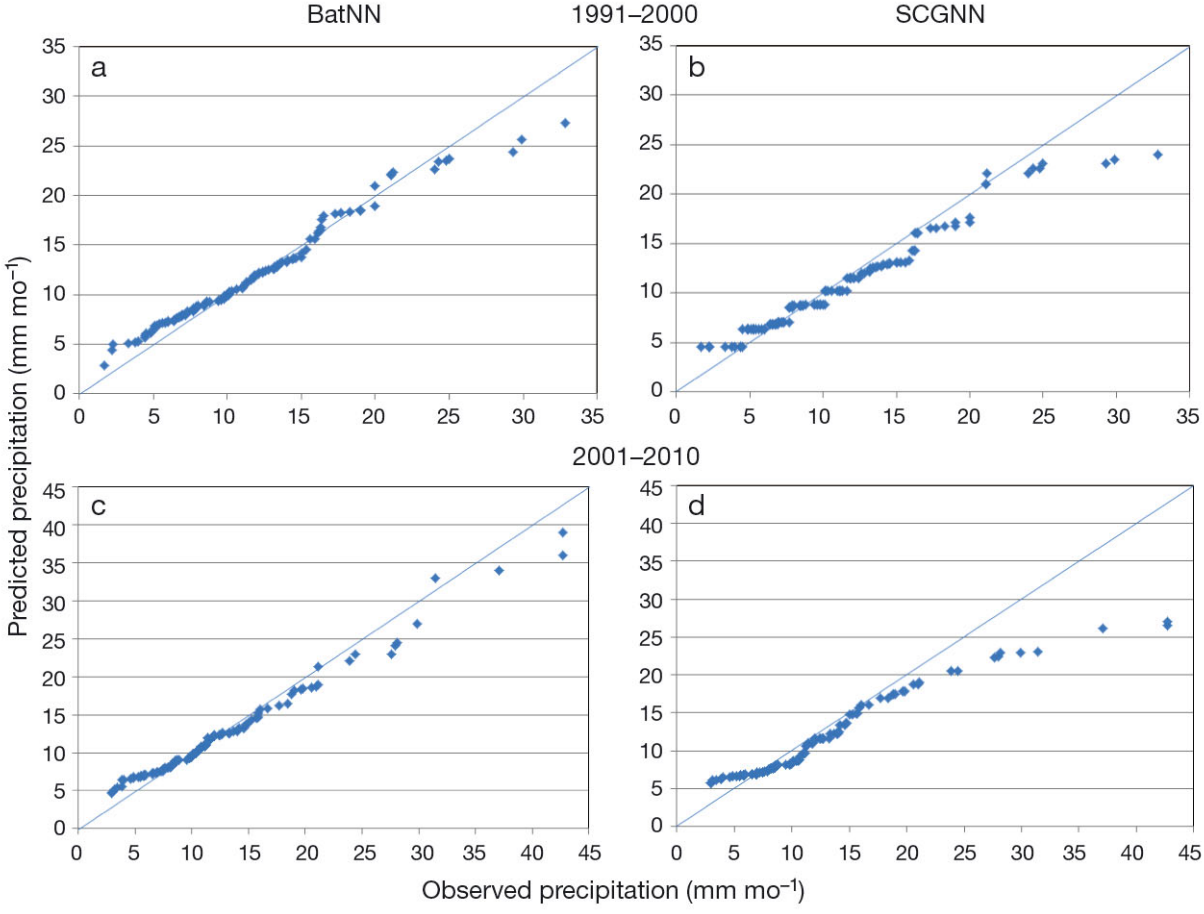

Fig. 6. QQ-plots of predicted against observed mean monthly precipitation from 1991 to 2000 and 2001 to 2010, simulated by (a,c) BatNN and (b,d) SCGNN (scaled conjugate gradient neural network)

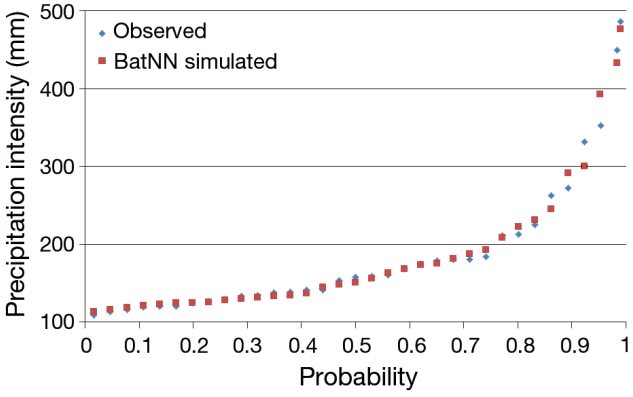

Fig. 7. Quantile plot of BatNN-downscaled daily annual maximum precipitation (AMP) and observed daily AMP in Kuching from 1961 to 2010

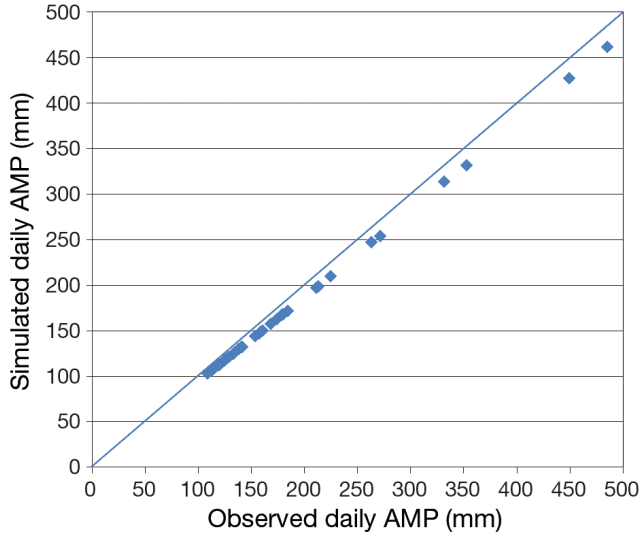

Fig. 8. QQ-plot of simulated daily annual maximum precipitation (AMP) against observed daily AMP in Kuching from 1961 to 2010

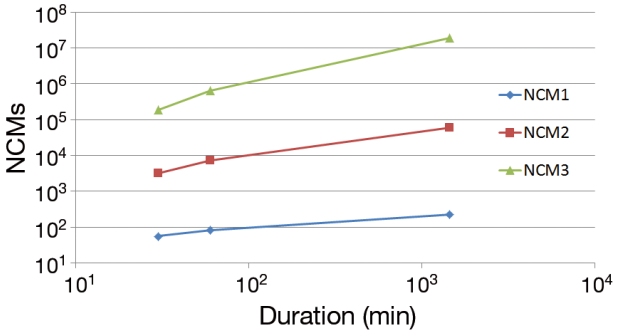

Fig. 9. Log-log plots of the first 3 orders of non-central moments (NCMs)

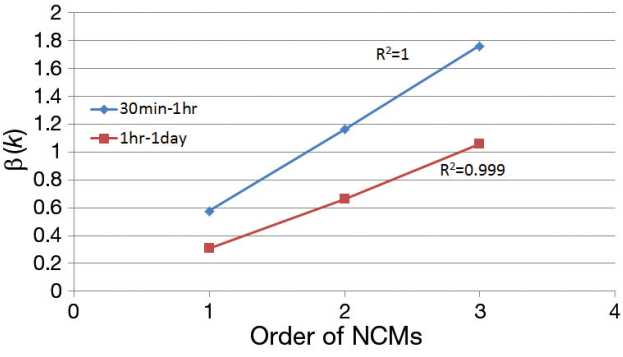

Fig. 10. Plot of scaling exponent β(k) versus order of non-central moments (NCMs)

tions. It can be observed that the NCMs display 2 distinct linear trends between 30 min and 1 h; and between 1 and 24 h, which implies that the AMP at these different time scales can be described in linear terms. In addition, the linear relationship of the scaling exponent, β(k) and the order of NCMs shown in Fig. 10 confirmed that the Kuching AMP quantiles from different durations can be estimated through the scaling-GEV approach.

In order to evaluate the feasibility of the NCM GEV and scaling-GEV methods, QQ-plots of AMP quantiles estimated using the Gumbel, NCM GEV and scaling-GEV methods, respectively, were plotted against observed AMP quantiles from different durations for Kuching in 1961 to 1990 . The Gumbel distribution has been used in Kuching for flood risk analyses and assessments (Daud et al. 2002, Ibrahim 2004).

As shown in Fig. 11, the NCM GEV and scaling-GEV methods are comparable to the Gumbel distribution method for AMP quantiles under 24 h. In particular, the Gumbel and NCM GEV methods were found to underestimate extreme precipitation, while scaling-GEV showed overestimation of extremes for AMP quantiles under 24 h (Fig. 11a–e). For AMPs over 24 h, the NCM GEV method displayed the tendency to underestimate precipitation of higher intensity, while overestimating precipitation of lower intensity, as shown in Fig. 11f,g. On the other hand, the scaling-GEV method displayed overestimation of higher intensity precipitation and underestimation of lower intensity precipitation. The Gumbel distribution showed a 'middle-of-the-road' performance.

3.4. Projections of future AMP and IDF curves

Fig. 12 shows the plots of AMP series for the 2020s, 2050s and 2080s. It can be seen that the predicted future AMPs showed a slight increase in intensity for precipitation <350 mm. For precipitation intensities

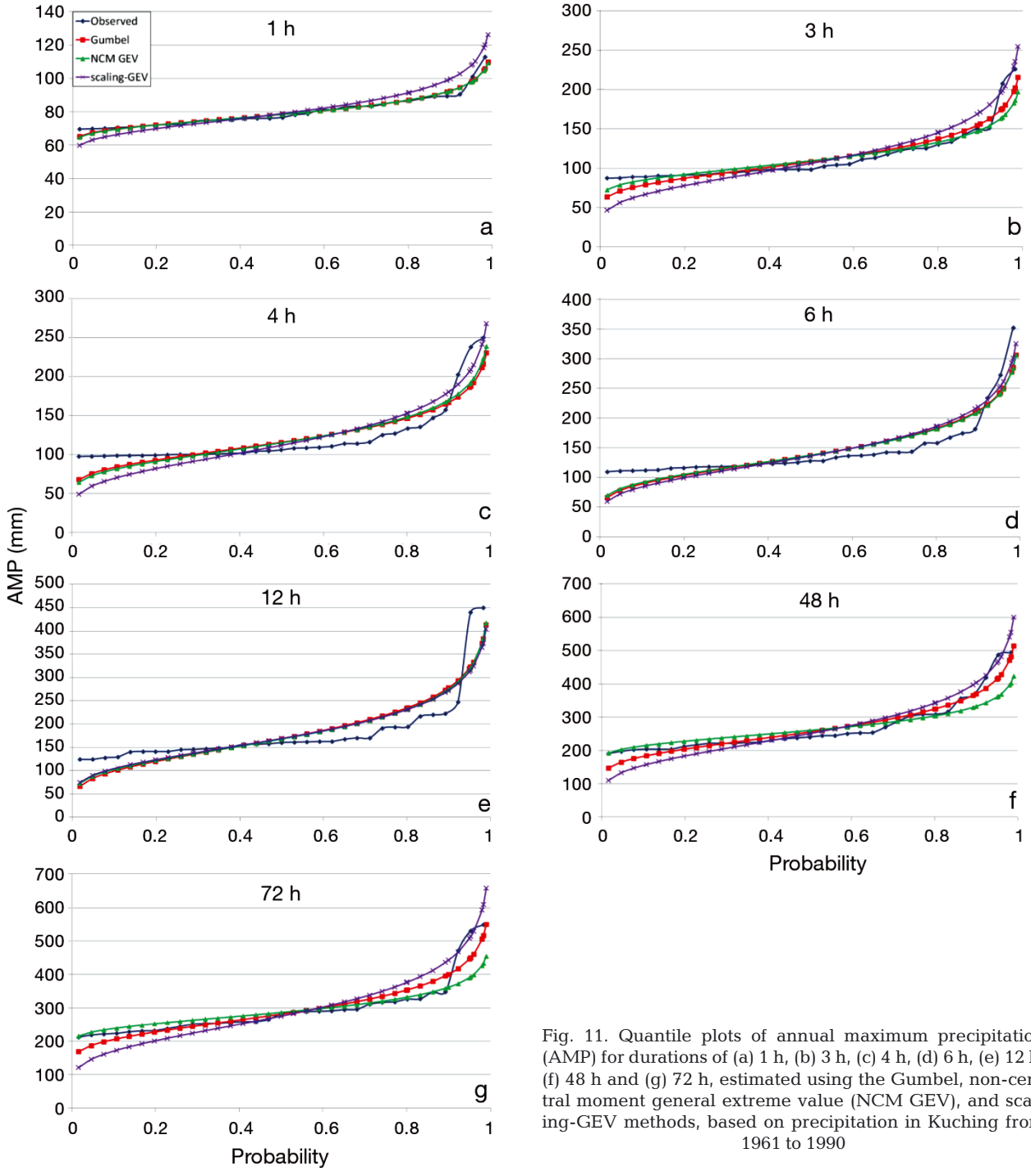

Fig. 11. Quantile plots of annual maximum precipitation (AMP) for durations of (a) 1 h, (b) 3 h, (c) 4 h, (d) 6 h, (e) 12 h, (f) 48 h and (g) 72 h, estimated using the Gumbel, non-central moment general extreme value (NCM GEV), and scaling-GEV methods, based on precipitation in Kuching from 1961 to 1990

>350 mm, higher extreme values were predicted, especially during the 2080s where the extreme precipitation was 19% more than during the 1970s. Overall, this result is consistent with the simulated precipitation change compiled by IPCC (2013) in AR5, where the average precipitation increase within the region is in the range of 0 to 10%, as forecasted by an ensemble of 39 models. Fig. 13 shows the predicted future IDF curves for the 2020s, 2050s and 2080s, respectively. The curves were constructed using simulated daily AMP series and the scaling-GEV method discussed in Section 2.5.

A comparison of trend changes in the predicted future IDF curves for each return period is shown in Fig. 14. It can be seen that the curves for the 2020s, 2050s and 2080s are closely matched to each other,

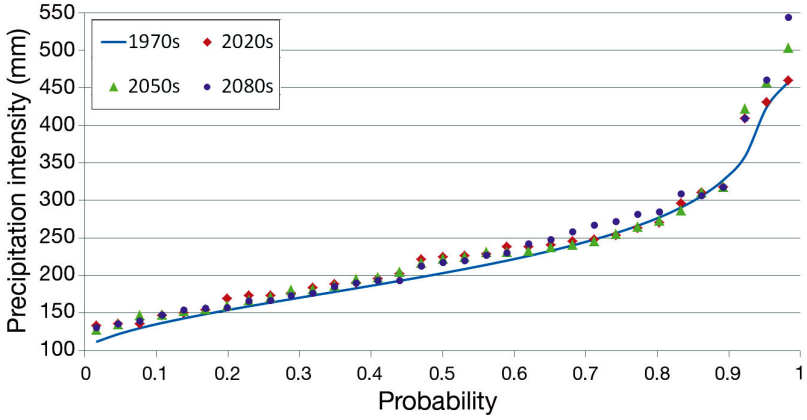

Fig. 12. Quantile plots of annual maximum precipitation (AMP) in the 1970s and BatNN-predicted AMPs for the 2020s, 2050s and 2080s based on ECHAM5 SRES A2

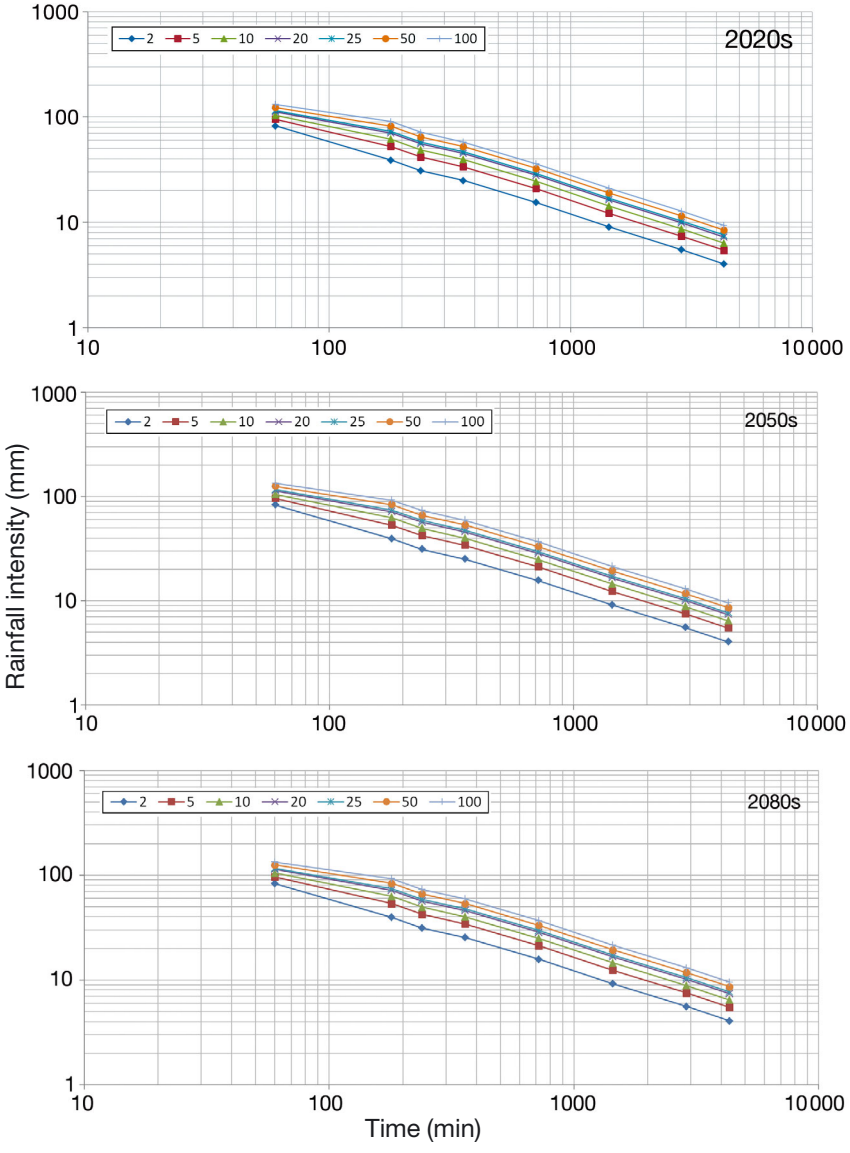

Fig. 13. Intensity-duration-frequency (IDF) curves for the 2020s, 2050s and 2080s based on ECHAM5 SRES A2

implying that there will not be any major shift in precipitation trend during these periods. When compared to the curves of the 1970s, there is a clear upward shift in all future average recurrence interval periods, which signifies higher precipitation intensity.

4. CONCLUSIONS

The present study proposes a spatial-temporal downscaling approach to solve the problem of predicting future precipitation in space and time. For spatial downscaling, the bat neural network (BatNN), a downscaling tool which combines an artificial neural network (ANN) and the bat algorithm (BA), is proposed. Its role is to downscale global climate predictors of GCM into local-scale climate conditions via a regression method. This was done by training the proposed model with observed precipitation and GCM predictors from 1961 to 1990. The trained model could then make predictions relating to future local precipitation by downscaling future GCM predictors.

The studied site is Kuching, where the annual total precipitation volume is >4000 mm. ECHAM5 SRES A2 was selected as the predicting emission scenario for this study. In order to evaluate the feasibility of the proposed downscaling model, predictions by BatNN and its benchmark SCGNN for precipitation in 1991 to 2010 were compared. The comparison revealed that BatNN has better predicting accuracy than its benchmark. However, both models displayed underestimation of higher intensity precipitation. The underestimation was more profound in SCGNN. It is important to note that BatNN holds an advantage over SCGNN because it does not share the weakness of this traditional gradient-descent optimisation method, which has been reported to be vulnerable to local optima trappings.

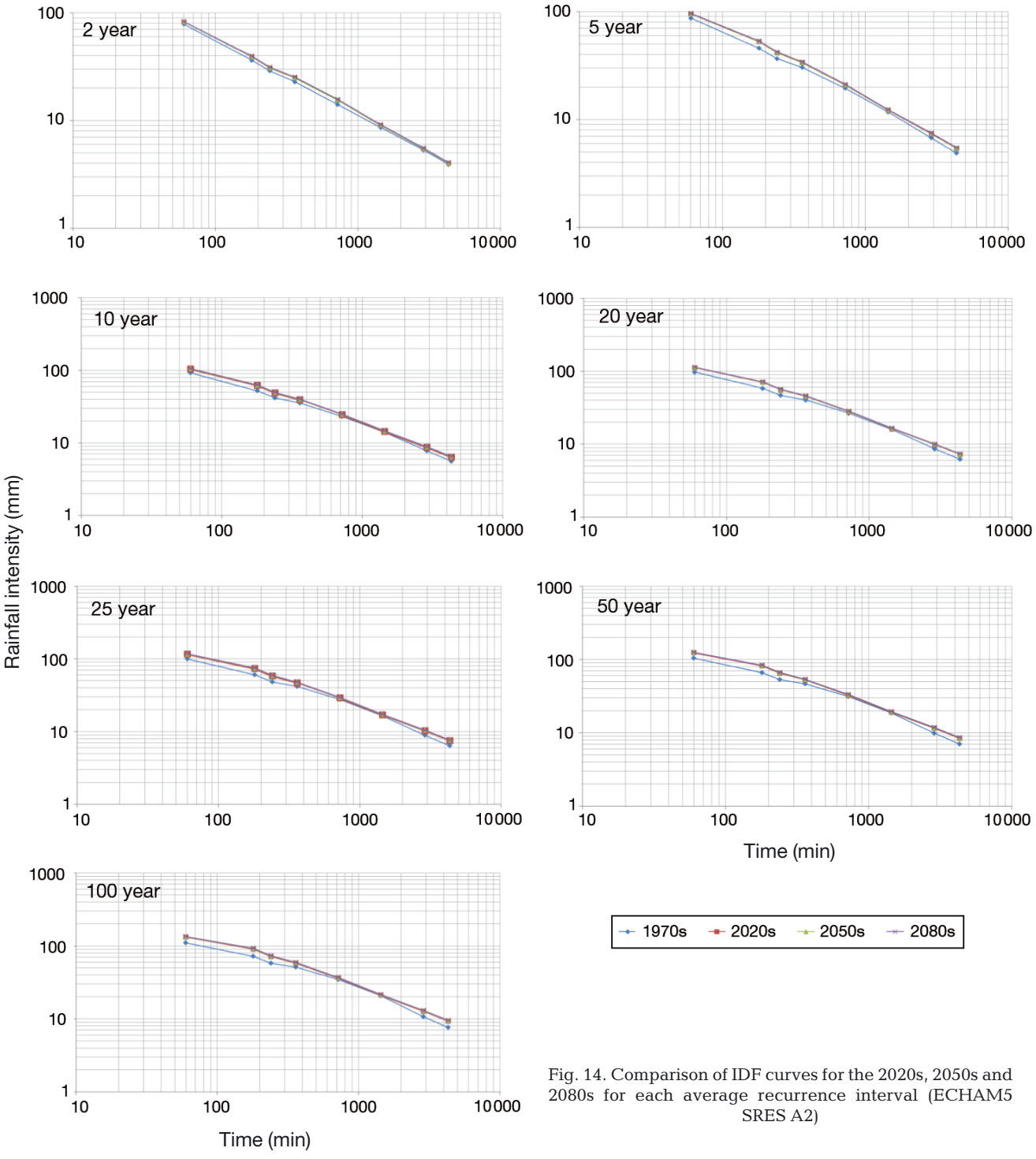

Fig. 14. Comparison of IDF curves for the 2020s, 2050s and 2080s for each average recurrence interval (ECHAM5 SRES A2)

The scaling-GEV approach is proposed for temporal downscaling. This approach is based on the concept of scale-invariance between daily and sub-daily precipitation quantiles, in which the statistical properties of the GEV distributions between the 2 time scales can be related via a simple scaling technique. It was found that the Kuching daily precipitation series had a simple linear relationship with its shorter and longer duration (1 to 72 h) precipitation quantiles. This approach was evaluated and found to be in good agreement with the currently used Gumbel distribution method.

Finally, future IDF curves for Kuching were projected for the 2020s, 2050s and 2080s using ECHAM5

SRES A2 predictors. The predicted AMP at the studied site was found to be generally higher than that of the base period (1961 to 1990). Furthermore, the projections revealed that there will be higher extremes, approximately 19% higher than the extremes found in the 1970s. An important point to note regarding precipitation forecasting is that it is sensitive to the bias of the underlying GCM (Wilby & Wigley 1997) and normalisation of its predictors due to coarse resolution. For example, some local climate variables and orography are averaged across a particular GCM grid box, leading to underestimation of climate characteristics (especially the extremes) of a particular local area. Consequently, GCMs have been regarded as incompetent in resolving circulation patterns that involve hydrological extremes (Christensen & Christensen 2003). It is also important to mention that analysis from one particular GCM is not very robust, and future work will attempt to incorporate more GCMs and even RCMs. Other GCMs were not included in this analysis as the objectives of this study were the development of BatNN for spatial downscaling of precipitation and the construction of future IDF curves in the context of climate change.

The findings of this study show that the proposed spatial-temporal downscaling method can be used as an alternative tool for estimating future precipitation trends under climate change scenarios. It is hoped that the present study can provide valuable insights for policymakers regarding the impact of climate change in urban areas. For further research, other metaheuristic algorithms, such as firefly and bee colony, can be adapted into ANNs. Moreover, the proposed BatNN and scaling-GEV can also be adapted for the prediction of other climate variables, such as temperature, humidity and sea level pressure, and for use in other regions.

LITERATURE CITED

Abdel-Rahman EM, Ahmad AR, Akhtar S (2012) A metaheuristic bat-inspired algorithm for full body human pose estimation. Ninth Conference on Computer and Robot Vision, 28–30 May 2012, Toronto, ON, p 369–375

Alam MS, Elshorbagy A (2015) Quantification of the climate change-induced variations in intensity–duration–frequency curves in the Canadian Prairies. J Hydrol (Amst) 527:990–1005

Arnbjerg-Nielsen K (2012) Quantification of climate change effects on extreme precipitation used for high resolution hydrologic design. Urban Water J 9:57–65

Bárdossy A, Stehlík J, Caspary HJ (2002) Automated objective classification of daily circulation patterns for precipitation and temperature downscaling based on optimized fuzzy rules. Clim Res 23:11–22

Barnett TP, Preisendorfer R (1987) Origins and levels of monthly and seasonal forecast skill for United States surface air temperatures determined by canonical correlation analysis. Mon Weather Rev 115:1825–1850

Blum C, Roli A (2003) Metaheuristics in combinatorial optimization: overview and conceptual comparison. ACM Comput Surv 35:268–308

Caesar J, Lowe JA (2012) Comparing the impacts of mitigation versus non-intervention scenarios on future temperature and precipitation extremes in the HadGEM2 climate model. J Geophys Res Atmos 117:1–14

Cheng CS, Li G, Li Q, Auld H (2008) Statistical downscaling of hourly and daily climate scenarios for various meteorological variables in south-central Canada. Theor Appl Climatol 91:129–147

Christensen JH, Christensen OB (2003) Climate modelling: severe summertime flooding in Europe. Nature 421: 805–806

Conway D, Wilby RL, Jones P (1996) Precipitation and air flow indices over the British Isles. Clim Res 7:169–183

Daud ZM, Kassim AHM, Desa MNM, Nguyen VTV (2002) Statistical analysis of at-site extreme rainfall processes in peninsular Malaysia. Int Assoc Hydrol Sci 274:61–68

Dawson CW, Wilby R (1998) An artificial neural network approach to rainfall-runoff modelling. Hydrol Sci J 43: 47–66

Diaz-Nieto J, Wilby RL (2005) A comparison of statistical downscaling and climate change factor methods: impacts on low flows in the River Thames, United Kingdom. Clim Change 69:245–268

Dibike YB, Gachon P, St-Hilaire A, Ouarda TBMJ, Nguyen VTV (2008) Uncertainty analysis of statistically downscaled temperature and precipitation regimes in Northern Canada. Theor Appl Climatol 91:149–170

Donat MG, Alexander LV, Yang H, Durre I and others (2013) Updated analyses of temperature and precipitation extreme indices since the beginning of the twentieth century: the HadEX2 dataset. J Geophys Res Atmos 118: 2098–2118

Fister I Jr, Fister D, Yang XS (2013) A hybrid bat algorithm. Elektrotehniški Vestnik 80:1–7

Flood I, Kartam N (1994) Neural networks in civil engineering I: principles and understanding. J Comput Civ Eng 8: 131–148

Fowler HJ, Wilby RL (2007) Beyond the downscaling comparison study. Int J Climatol 27:1543–1545

Fowler HJ, Kilsby CG, O'Connell PE (2000) A stochastic rainfall model for the assessment of regional water resource systems under changed climatic condition. Hydrol Earth Syst Sci Discuss 4:263–281

Fowler HJ, Blenkinsop S, Tebaldi C (2007) Linking climate change modelling to impacts studies: Recent advances in downscaling techniques for hydrological modelling. Int J Climatol 27:1547–1578

Frei C, Schöll R, Fukutome S, Schmidli J, Vidale PL (2006) Future change of precipitation extremes in Europe: intercomparison of scenarios from regional climate models. J Geophys Res Atmos 111:D06105, doi:10.1029/2005JD005965

French MN, Krajewski WF, Cuykendall RR (1992) Rainfall forecasting in space and time using a neural network. J Hydrol (Amst) 137:1–31

Gandomi AH, Yang XS, Talatahari S, Alavi AH (2013) Metaheuristic algorithms in modelling and optimization. In: Gadomi AH, Yang XS, Talatahari S, Alavi AH (eds)

Metaheuristic applications in structures and infrastructures. Elsevier, Oxford, p 1–24

Goodess CM, Palutikof JP (1998) Development of daily rainfall scenarios for south east Spain using a circulation-type approach to downscaling. Int J Climatol 18: 1051–1083

Gorp J, Schoukens J, Pintelon R (1998) Adding input noise to increase the generalization of neural networks is a bad idea. Proc Artificial Neural Networks in Engineering Conf, ANNIE 98, St. Louis, MO, 1–4 November 1998. 8: 127–132

Gupta VK (2004) Emergence of statistical scaling in floods on channel networks from complex runoff dynamics. Chaos Solitons Fractals 19:357–365

Gupta VK, Waymire E (1990) Multiscaling properties of spatial rainfall and river flow distributions. J Geophys Res Atmos 95:1999–2009

Gutiérrez JM, San-Martín D, Brands S, Manzanas R, Herrera S (2013) Reassessing statistical downscaling techniques for their robust application under climate change conditions. J Clim 26:171–188

Hailegeorgis TT, Thorolfsson ST, Alfredsen K (2013) Regional frequency analysis of extreme precipitation with consideration of uncertainties to update IDF curves for the city of Trondheim. J Hydrol (Amst) 498:305–318

Hartmann DJ, Klein Tank AMG, Rusticucci M, Alexander LV and others (2013) Observations: atmosphere and surface. In: Stocker TF, Qin D, Plattner GK, Tignor M and others (eds) Climate change 2013: the physical science basis. Contribution of Working Group I to the Fifth Assessment Report of the Intergovernmental Panel on Climate Change. Cambridge University Press, Cambridge and New York

Hashmi MZ, Shamseldin AY, Melville BW (2011) Comparison of SDSM and LARS-WG for simulation and downscaling of extreme precipitation events in a watershed. Stochastic Environ Res Risk Assess 25:475–484

Hassoun MH (1995) Fundamentals of artificial neural networks. MIT Press, Cambridge

Haylock MR, Cawley GC, Harpham C, Wilby RL, Goodess CM (2006) Downscaling heavy precipitation over the United Kingdom: a comparison of dynamical and statistical methods and their future scenarios. Int J Climatol 26: 1397–1416

Huth R, Kyselý J, Dubrovský M (2001) Time structure of observed, GCM-simulated, downscaled, and stochastically generated daily temperature series. J Clim 14: 4047–4061

Ibrahim I (2004) Identification of a probability distribution for extreme rainfall series in East Malaysia. Masters thesis, Kolej Universiti Teknologi Tun Hussein Onn, Bahu Pahat

IPCC (2011) Frequently asked questions. Intergovernmental Panel on Climate Change (IPCC), www.ipcc-data.org/ddc_faqs.html, viewed 15 February 2013

IPCC (2013) Summary for policymakers. In: Stocker TF, Qin D, Plattner GK, Tignor M and others (eds) Climate change 2013: the physical science basis. Contribution of Working Group I to the Fifth Assessment Report of the Intergovernmental Panel on Climate Change. Cambridge University Press, Cambridge

Karamouz M, Fallahi M, Nazif S, Farahani MR (2009) Long lead rainfall prediction using statistical downscaling and artificial neural network modeling. Transaction A. Civ Eng 16:165–172

Kuligowski R, Barros A (1998) Localized precipitation forecasts from a numerical weather prediction model using artificial neural networks. Weather Forecast 13:1194–1204

Lachtermacher G, Fuller JD (1994) Backpropagation in hydrological time series forecasting. In: Hipel KW, McLeod AI, Panu US, Singh VP (eds) Stochastic and statistical methods in hydrology and environmental engineering. Water Science and Technology Library, Vol 10/3. Kluwer Academic Publishers, Dordrecht, p 229–242

Levenberg K (1944) A method for the solution of certain non-linear problems in least squares. Q Appl Math 2: 164–168

Lin J, Chou C, Yang C, Tsai H (2012) A chaotic Levy flight bat algorithm for parameter estimation in nonlinear dynamic biological systems. J Comput Inf Technol 2: 56–63

Luk KC, Ball JE, Sharma A (2000) A study of optimal model lag and spatial inputs to artificial neural network for rainfall forecasting. J Hydrol (Amst) 227:56–65

Maier HR, Dandy GC (2000) Neural networks for the prediction and forecasting of water resources variables: a review of modelling issues and applications. Environ Model Softw 15:101–124

Maraun D (2012) Nonstationarities of regional climate model biases in European seasonal mean temperature and precipitation sums. Geophys Res Lett 39:L06706, doi: 10.1029/2012GL051210

Maraun D (2013) Bias correction, quantile mapping, and downscaling: revisiting the inflation issue. J Clim 26: 2137–2143

Maraun D, Wetterhall F, Ireson AM, Chandler RE and others (2010) Precipitation downscaling under climate change: recent developments to bridge the gap between dynamical models and the end user. Rev Geophys 48:RG3003, doi:10.1029/2009RG000314

Maren A, Harston C, Pap R (1990) Handbook of neural computing applications. Academic Press, San Diego, CA

Marquardt D (1963) An algorithm for least-squares estimation of nonlinear parameters. J Soc Ind Appl Math 11: 431–441

Marzban C, Stumpf GJ (1996) A neural network for tornado prediction based on Doppler radar-derived attributes. J Appl Meteorol 35:617–626

Masters T (1993) Practical neural network recipes in C++. Academic Press, San Diego, CA

Malaysian Meteorological Department (MMD) (2009) Climate change scenarios for Malaysia 2001–2099. Numerical Weather Prediction Development Section, Technical Development Division, Malaysian Meteorological Department (MMD), Ministry of Science, Technology and Innovation, Malaysia

Møhl B (1988) Target detection by echolocating bats. In: Nachtigall PE, Moore PWB (eds) Animal sonar: processes and performance. Plenum Press, New York, p 435–450

Møller M (1993) A scaled conjugate gradient algorithm for fast supervised learning. Neural Netw 6:525–533

MOSTI (Ministry of Science, Technology and Innovation) (2013) Seasonal rainfall variation in Sabah and Sarawak. Ministry of Science, Technology and Innovation, Putrajaya

Musikapun P, Pongcharoen P (2012) Solving multi-stage multi-machine multi-product scheduling problem using bat algorithm. Second Int Conf Management and Artifi-

cial Intelligence (IPEDR). IASCIT Press, Singapore, 35: 98–102

Nakicenovic N, Swart R (eds) (2000) Special report on emissions scenarios. Cambridge University Press, Cambridge

Nguyen VTV, Nguyen T, Ashkar F (2002) Regional frequency analysis of extreme rainfalls. Water Sci Technol 45:75–81

Nguyen VTV, Nguyen TD, Cung A (2007) A statistical approach to downscaling of sub-daily extreme rainfall processes for climate-related impact studies in urban areas. Water Sci Technol Water Supply 7:183–192

Nguyen VTV, Desramaut N, Nguyen TD (2008) Estimation of urban design storms in consideration of GCM-based climate change scenarios. In: Feyen J, Shannon K, Neville M (eds) Water and urban development paradigms: towards an integration of engineering, design and management approaches. Taylor and Francis, London, p 347–356.

Orlowsky B, Seneviratne SI (2012) Global changes in extreme events: regional and seasonal dimension. Clim Change 110:669–696

Ramesh B, Mohan VCJ, Reddy VCV (2013) Application of bat algorithm for combined economic load and emission dispatch. Int J Electr Electron Eng Telecommun 2:1–9

Richardson P (2008) Bats. Natural History Museum, London

Rodríguez R, Navarro X, Casas MC, Ribalaygua J, Russo B, Pouget L, Redaño A (2014) Influence of climate change on IDF curves for the metropolitan area of Barcelona (Spain). Int J Climatol 34:643–654

Roeckner E, Bäuml G, Bonaventura L, Brokopf R and others (2003) The atmospheric general circulation model ECHAM5. 1. Model description. Report No. 349. Max Planck Institute for Meteorology, Hamburg

Rojas R (1996) Neural networks: a systematic introduction. Springer-Verlag, Berlin

Sailor DJ, Hu T, Li X, Rosen JN (2000) A neural network approach to local downscaling of GCM output for assessing wind power implications of climate change. Renew Energy 19:359–378

Salathe EP, Mote PW, Wiley MW (2007) Review of scenario selection and downscaling methods for the assessment of climate change impacts on hydrology in the United States pacific northwest. Int J Climatol 27:1611–1621

Schoof JT, Robeson SM (2015) Projecting changes in regional temperature and precipitation extremes in the United States. Weather Clim Extremes 11:28–40

Semenov MA, Barrow EM (1997) Use of a stochastic weather generator in the development of climate change scenarios. Clim Change 35:397–414

Sillmann J, Kharin VV, Zwiers FW, Zhang X, Bronaugh D (2013) Climate extremes indices in the CMIP5 multimodel ensemble. 2. Future climate projections. J Geophys Res Atmos 118:2473–2493

Silverman D, Dracup JA (2000) Artificial neural networks and long-range precipitation prediction in California. J Appl Meteorol 39:57–66

Solaiman TA, Simonovic SP (2011) Development of probability based intensity-duration-frequency curves under climate change. Water Resources Research Report, Department of Civil and Environmental Engineering, University of Western Ontario, London

Sunyer MA, Madsen H, Ang PH (2012) A comparison of different regional climate models and statistical downscaling methods for extreme rainfall estimation under climate change. Atmos Res 103:119–128

Surlykke A, Boel Pedersen S, Jakobsen L (2009) Echolocating bats emit a highly directional sonar sound beam in the field. Proc R Soc B 276:853–860

Valipour M (2015a) Future of agricultural water management in Africa. Arch Agron Soil Sci 61:907–927

Valipour M (2015b) A comprehensive study on irrigation management in Asia and Oceania. Arch Agron Soil Sci 61:1247–1271

Valverde Ramírez MC, de Campos Velho HF, Ferreira NJ (2005) Artificial neural network technique for rainfall forecasting applied to the São Paulo region. J Hydrol (Amst) 301:146–162

Viswanathan GM, Afanasyev V, Buldyrev SV, Murphy EJ, Prince PA, Stanley HE (1996) Lévy flight search patterns of wandering albatrosses. Nature 381:413–415

Wetterhall F, Bárdossy A, Chen D, Halldin S, Xu CY (2006) Daily precipitation downscaling techniques in three Chinese regions. Water Resour Res 42:W11423, doi:10.1029/2005WR004573

Wilby RL, Dawson CW (2013) The statistical downscaling model: insights from one decade of application. Int J Climatol 33:1707–1719

Wilby RL, Harris I (2006) A framework for assessing uncertainties in climate change impacts: low flow scenarios for the River Thames, UK. Water Resour Res 42:W02419, doi: 10.1029/2005WR004065

Wilby RL, Wigley TML (1997) Downscaling general circulation model output: a review of methods and limitations. Prog Phys Geogr 21:530–548

Wilby RL, Wigley TML (2000) Precipitation predictors for downscaling: observed and general circulation model relationships. Int J Climatol 20:641–661

Wilby RL, Dawson CW, Barrow EM (2002) SDSM — a decision support tool for the assessment of regional climate change impacts. Environ Model Softw 17:145–157

Wilby RL, Tomlinson OJ, Dawson CW (2003) Multi-site simulation of precipitation by conditional resampling. Clim Res 23:183–194

Wilby RL, Whitehead PG, Wade AJ, Butterfield D, Davis RJ, Watts G (2006) Integrated modelling of climate change impacts on water resources and quality in a lowland catchment: River Kennet, UK. J Hydrol (Amst) 330:204–220

Willems P, Vrac M (2011) Statistical precipitation downscaling for small-scale hydrological impact investigations of climate change. J Hydrol (Amst) 402:193–205

Yang XS (2010) A new metaheuristic bat-inspired algorithm. In: González JR, Pelta DA, Cruz C, Terrazas G, Krasnogor N (eds) Nature inspired cooperative strategies for optimization (NICSO 2010). Springer-Verlag, Berlin, p 65–74

Yang XS (2011) Bat algorithm for multi-objective optimisation. Int J Bio-Inspired Comput 3:267–274

Yang XS (2012) Metaheuristic optimization with applications: demonstration via bat algorithm. In: B Filipic, J Silc (eds) Proc 5th Bioinspired optimization methods and their applications (BIOMA2012), 24–25 May 2012, Bohini, Slovenia, p 23–34

Yang XS (2013) Bat algorithm: literature review and applications. Int J Bio-inspired Comput 5:141–149

Yang XS, Gandomi AH (2012) Bat algorithm: a novel approach for global engineering optimization. Eng Comput 29:464–483

Yang XS, Gandomi AH, Talatahari S, Alavi AH (eds) (2012) Metaheuristics in water, geotechnical and transport engineering. Elsevier, London

Editorial responsibility: Gouyu Ren, Beijing, China

Submitted: October 20, 2015; Accepted: February 22, 2016
Proofs received from author(s): April 6, 2016